

Investigating the peculiar emission from the new VHE gamma-ray source H1722+119

M. L. Ahnen¹, S. Ansoldi², L. A. Antonelli³, P. Antoranz⁴, A. Babic⁵, B. Banerjee⁶, P. Bangale⁷, U. Barres de Almeida^{7,24}, J. A. Barrio⁸, J. Becerra González^{9,25}, W. Bednarek¹⁰, E. Bernardini^{11,26}, B. Biasuzzi², A. Biland¹, O. Blanch¹², S. Bonnefoy⁸, G. Bonnoli³, F. Borracci⁷, T. Bretz^{13,27}, S. Buson¹⁴, A. Carosi³, A. Chatterjee⁶, R. Clavero⁹, P. Colin⁷, E. Colombo⁹, J. L. Contreras⁸, J. Cortina¹², S. Covino³, P. Da Vela⁴, F. Dazzi⁷, A. De Angelis¹⁴, B. De Lotto², E. de Oña Wilhelmi¹⁵, F. Di Pierro³, M. Doert¹⁶, A. Domínguez⁸, D. Dominis Prester⁵, D. Dorner¹³, M. Doro¹⁴, S. Einecke¹⁶, D. Eisenacher Glawion¹³, D. Elsaesser¹⁶, V. Fallah Ramazani¹⁷, A. Fernández-Barral¹², D. Fidalgo⁸, M. V. Fonseca⁸, L. Font¹⁸, K. Frantzen¹⁶, C. Fruck⁷, D. Galindo¹⁹, R. J. García López⁹, M. Garczarczyk¹¹, D. Garrido Terrats¹⁸, M. Gaug¹⁸, P. Giammaria³, N. Godinović⁵, A. González Muñoz¹², D. Gora¹¹, D. Guberman¹², D. Hadasch²⁰, A. Hahn⁷, Y. Hanabata²⁰, M. Hayashida²⁰, J. Herrera⁹, J. Hose⁷, D. Hrupec⁵, G. Hughes¹, W. Idec¹⁰, K. Kodani²⁰, Y. Konno²⁰, H. Kubo²⁰, J. Kushida²⁰, A. La Barbera³, D. Lelas⁵, E. Lindfors¹⁷, S. Lombardi³, F. Longo², M. López⁸, R. López-Coto¹², P. Majumdar⁶, M. Makariev²¹, K. Mallot¹¹, G. Maneva²¹, M. Manganaro⁹, K. Mannheim¹³, L. Maraschi³, B. Marcote¹⁹, M. Mariotti¹⁴, M. Martínez¹², D. Mazin^{7,20}, U. Menzel⁷, J. M. Miranda⁴, R. Mirzoyan⁷, A. Moralejo¹², E. Moretti⁷, D. Nakajima²⁰, V. Neustroev¹⁷, A. Niedzwiecki¹⁰, M. Nieves Rosillo⁸, K. Nilsson^{17,28}, K. Nishijima²⁰, K. Noda⁷, L. Nogués¹², R. Orito²⁰, A. Overkemping¹⁶, S. Paiano¹⁴, J. Palacio¹², M. Palatiello², D. Paneque⁷, R. Paoletti⁴, J. M. Paredes¹⁹, X. Paredes-Fortuny¹⁹, G. Pedalletti¹¹, L. Perri³, M. Persic^{2,29}, J. Poutanen¹⁷, P. G. Prada Moroni²², E. Prandini^{1,30}, I. Puljak⁵, W. Rhode¹⁶, M. Ribó¹⁹, J. Rico¹², J. Rodriguez Garcia⁷, T. Saito²⁰, K. Satalecka¹¹, C. Schultz¹⁴, T. Schweizer⁷, A. Sillanpää¹⁷, J. Sitarek¹⁰, I. Snidarić⁵, D. Sobczynska¹⁰, A. Stamerra³, T. Steinbring¹³, M. Strzys⁷, L. Takalo¹⁷, H. Takami²⁰, F. Tavecchio³, P. Temnikov²¹, T. Terzić^{5*}, D. Tescaro¹⁴, M. Teshima^{7,20}, J. Thaele¹⁶, D. F. Torres²³, T. Toyama⁷, A. Treves², V. Verguilov²¹, I. Vovk⁷, J. E. Ward¹², M. Will⁹, M. H. Wu¹⁵, R. Zanin¹⁹ (The MAGIC Collaboration), F. D'Ammando^{31,32} (for the *Fermi*-LAT Collaboration), T. Hovatta^{33,34}, W. Max-Moerbeck³⁵, C. M. Raiteri³⁶, A. C. S. Readhead³⁴, R. Reinthal³⁷, J. L. Richards³⁸, F. Verrecchia^{39,40} and M. Villata³⁶

(Affiliations can be found after the references)

Accepted XXX. Received YYY; in original form ZZZ

ABSTRACT

The MAGIC (Major Atmospheric Gamma-ray Imaging Cherenkov) telescopes observed the BL Lac object H1722+119 (redshift unknown) for six consecutive nights between 2013 May 17 and 22, for a total of 12.5 h. The observations were triggered by high activity in the optical band measured by the KVA (Kungliga Vetenskapsakademien) telescope. The source was for the first time detected in the very high energy (VHE, $E > 100$ GeV) γ -ray band with a statistical significance of 5.9σ . The integral flux above 150 GeV is estimated to be (2.0 ± 0.5) per cent of the Crab Nebula flux. We used contemporaneous high energy (HE, $100 \text{ MeV} < E < 100 \text{ GeV}$) γ -ray observations from *Fermi*-LAT (Large Area Telescope) to estimate the redshift of the source. Within the framework of the current extragalactic background light models, we estimate the redshift to be $z = 0.34 \pm 0.15$. Additionally, we used contemporaneous X-ray to radio data collected by the instruments on board the *Swift* satellite, the KVA, and the OVRO (Owens Valley Radio Observatory) telescope to study multifrequency characteristics of the source. We found no significant temporal variability of the flux in the HE and VHE bands. The flux in the optical and radio wavebands, on the other hand, did vary with different patterns. The spectral energy distribution (SED) of H1722+119 shows surprising behaviour in the $\sim 3 \times 10^{14} - 10^{18}$ Hz frequency range. It can be modelled using an inhomogeneous helical jet synchrotron self-Compton model.

Key words: BL Lacertae objects: individual: H1722+119 – gamma-rays: galaxies – galaxies: active – galaxies: distances and redshifts

1 INTRODUCTION

Active galactic nuclei (AGN) are the most luminous persistent sources of electromagnetic radiation in the Universe. They are compact regions in the centres of galaxies formed around supermassive black holes (SMBHs) that actively accrete matter. Approximately 10 per cent of AGN eject matter through relativistic jets (Dunlop et al. 2003). AGN whose jets are oriented close to the line of sight to the Earth are referred to as blazars. Jets are sources of electromagnetic radiation of all wavelengths from radio to γ -rays. They can extend to Mpc distances from the nucleus and can be brighter than the rest of the galaxy. The spectral energy distribution (SED) of blazars is characterised by two broad peaks: a “low-energy” peak in the optical to X-ray band and a “high-energy” peak in the X-ray to γ -ray band. Their emission is characterised by the strong and variable linear polarisation in the optical and radio bands, and high variability in flux across the entire electromagnetic spectrum. Blazars can be divided into two classes according to the characteristics of their emission: flat spectrum radio quasars (FSRQs) and BL Lacertae objects (BL Lacs). FSRQs are known to have prominent broad and narrow optical emission lines, in addition to strong optical and X-ray continuum emission. A quite common feature is the so-called blue bump in the optical-UV band associated with the emission from the accretion disc. BL Lacs, on the other hand exhibit very weak optical emission lines if any at all. The low-energy peak in SED of FSRQs is believed to be a combination of synchrotron radiation of electrons in the jet and thermal emission from the broad line region (BLR), dust torus and

accretion disc, while usually in the case of BL Lacs, all the emission is attributed to synchrotron emission. According to leptonic scenarios, the second peak is a result of inverse Compton (IC) scattering of lower-energy photons (so-called seed photons) on relativistic electrons within the jet, while hadronic scenarios assume protons in the jet are accelerated even to energies $\gtrsim 10^{19}$ eV and significantly contribute to the emission either through proton-synchrotron emission in relatively strong magnetic fields, or photo-pion production (Böttcher et al. 2013). Ghisellini et al. (2010) showed that the broad-band SEDs of γ -ray blazars can be, on average, well described by a simple one-zone leptonic model including synchrotron and IC emission components, with the addition of possible external contributions from e.g. the accretion disc or host galaxy emission.

H1722+119 was first observed in the 1970s as a part of the *Uhuru* X-ray sky survey and the *HEAO 1* Large Area Sky Survey (LASS). The resulting X-ray source catalogues (Forman et al. (1978); source name: 4U1722+11, and Wood et al. (1984); source name: 1H1720+117) only identify it as an X-ray source. Almost twenty years later, Griffiths et al. (1989) and Brissenden et al. (1990) independently, classified it as a BL Lac object. Furthermore, H1722+119 was classified as an intermediate-energy-peaked BL Lac with the low-energy peak at $\nu_s = 6.3 \times 10^{15}$ Hz (Nieppola et al. 2006). Brissenden et al. (1990) measured a very high level of linear polarization in the optical band, reaching 17.6 ± 1.0 per cent in the B band. H1722+119 has been observed in the radio band by the OVRO (Owens Valley Radio Observatory) since 2007 (Richards et al. 2011)¹. H1722+119 is included in the third *Fermi*-LAT (Large Area Telescope) catalogue (3FGL; Acero et al. 2015) as a counterpart of the γ -ray source 3FGL J1725.0+1152, with photon index $\Gamma = 1.89 \pm 0.05$ and 0.1–100 GeV flux of

* Corresponding authors: T. Terzić, email: tterzic@phy.uniri.hr, A. Stamerra, email: stamerra@oato.inaf.it, F. D’Ammando, email: dammando@ira.inaf.it, C. M. Raiteri, email: raiteri@oato.inaf.it, F. Verrecchia, email: francesco.verrecchia@asdc.asi.it

¹ www.astro.caltech.edu/ovroblazars

$(2.7 \pm 0.3) \times 10^{-8} \text{ ph cm}^{-2} \text{ s}^{-1}$. Interesting studies, in which radio and high energy (HE, $100 \text{ MeV} < E < 100 \text{ GeV}$) γ -ray properties of blazars and their correlations are discussed, were presented in [Lister et al. \(2011\)](#) and [Linford et al. \(2012\)](#). Both works used the LAT on board the *Fermi Gamma-ray Space Telescope* for HE γ -ray and the Very Long Baseline Array for radio observations. [Linford et al. \(2012\)](#) (source name: F17250+1151) describe H1722+119 as a compact source with a short jet. Infrared (IR) observations of H1722+119 were performed as part of the Two Micron All-Sky Survey ([Mao 2011](#)). H1722+119 was listed as a candidate TeV blazar in [Costamante & Ghisellini \(2002\)](#) based on its X-ray and radio properties. Observations in the very high energy (VHE, $E > 100 \text{ GeV}$) γ -ray band were first reported in [Aleksić et al. \(2011, source name: RX J1725.0+1152\)](#). The MAGIC (Major Atmospheric Gamma-ray Imaging Cherenkov) telescope observed H1722+119 between 2005 and 2009 together with 20 other BL Lac candidates. H1722+119 was selected for this campaign based on its X-ray properties from [Donato et al. \(2001\)](#). The stacked sample of observed blazars showed a signal above 100 GeV with a significance of 4.9σ , but the analysis of H1722+119 data alone resulted in 1.4σ after 32 h of observation, with an upper limit (UL) of flux above 140 GeV of $1.3 \times 10^{-11} \text{ ph cm}^{-2} \text{ s}^{-1}$.

Although [Brissenden et al. \(1990\)](#) reported a featureless optical spectrum, [Griffiths et al. \(1989\)](#) estimated the redshift of the host galaxy based on an absorption feature to be $z = 0.018$. However, this result was not confirmed by other optical observations (e.g. [Véron-Cetty & Véron 1993](#); [Falomo et al. 1993, 1994](#)). [Sbarufatti et al. \(2006\)](#) observed H1722+119 with the ESO Very Large Telescope and detected no intrinsic features in the optical spectra. They derived a lower limit (LL) of $z > 0.17$. [Landoni et al. \(2014\)](#) used the spectrograph X-Shooter at the European Southern Observatory Very Large Telescope to set a LL on the redshift at 0.35. They detected no intrinsic or intervening spectral lines, ascribing this to extreme optical beaming, setting the ratio of beamed to thermal emission at ≥ 400 . [Farina et al. \(2013, priv. comm.\)](#) observed H1722+119 with the NOTCam of the Nordic Optical Telescope in the H-band in 2013 and were unable to detect the host galaxy. Applying the imaging redshift technique proposed by [Sbarufatti et al. \(2005\)](#), they set a LL on redshift at 0.4.

In this paper we report the first detection of VHE γ -ray emission from H1722+119, by the MAGIC telescopes ([Cortina 2013](#)), and study the multifrequency characteristics of H1722+119 in that period. Emission from blazars is quite variable in time, and optical high states are often used to trigger MAGIC observations. H1722+119 joins quite a long list of blazars, whose VHE γ -ray signal was detected following an optical high state (see e.g. [Albert et al. 2006, 2007b, 2008b](#); [Anderhub et al. 2009](#); [Aleksić et al. 2012b,c, 2014, 2015](#)). In Section 2 we present the instruments used in this work and their respective results. Section 3 is reserved for study of multifrequency characteristics. We summarise our findings in Section 4. Throughout the paper, we assume standard Λ CDM cosmology ([Komatsu et al. 2011](#)).

2 OBSERVATIONS AND DATA ANALYSIS

2.1 MAGIC

The MAGIC telescopes are located at the Observatorio del Roque de los Muchachos in the Canary Island of La Palma, Spain ($28^\circ 45'$ north, $18^\circ 54'$ west), at 2200 m above sea level. Two 17 m diameter Imaging Atmospheric Cherenkov Telescopes are optimised for observations of γ -rays of energies above 50 GeV . A detailed overview of the MAGIC experiment and the telescope performance is given in [Aleksić et al. \(2016a,b\)](#).

The results reported here are based on the observations performed during six nights between 2013 May 17 and 22, triggered by the high optical state detected by the KVA (Kungliga Vetenskaps Akademierteleskope) (see Section 2.4). Between the first (2005–2009) and the second (2013) observation campaign the MAGIC system underwent a series of major upgrades (see [Cortina et al. 2005](#); [Albert et al. 2008a](#); [Goebel et al. 2008](#); [Aleksić et al. 2012a](#); [Sitarek et al. 2013](#); [Aleksić et al. 2016a,b](#)). The current instrument is roughly twice as sensitive in the $100 - 200 \text{ GeV}$ energy range compared to the single MAGIC I telescope in operation in 2009 ([Aleksić et al. 2016b](#)).

MAGIC usually observes sources in the so called *wobble* mode ([Fomin et al. 1994](#); [Aleksić et al. 2016b](#)). H1722+119 was observed in four false-source positions for a total of 12.5 h during 2013. After quality selection based on the stability of the event rates, the effective time amounted to 12.0 h. Observations were performed at zenith angles between 16° and 37° .

The data were analysed within the MARS (MAGIC Analysis and Reconstruction Software) analysis framework ([Lombardi et al. 2011](#); [Zanin et al. 2013](#)). The VHE γ -ray signal is estimated using the distribution of the squared angular distance (θ^2) between the reconstructed and nominal (ON-source) source positions in the camera coordinates for each event. Background is estimated in the same manner with respect to the OFF-source position. Usually three OFF-source positions are chosen at the same distance from the camera centre as the ON-source position and rotated by 90° each. N_{on} is the number of events originating within the source region ($\theta^2 < 0.0125 \text{ deg}^2$), and N_{off} the normalised number of all events from the same region around OFF-source positions. An excess of 337.5 events above 60 GeV with respect to the background was detected, yielding a signal significance of 5.9σ using Eq. 17 of [Li & Ma \(1983\)](#). The θ^2 distribution is shown in Fig. 1. The light curve of the integral VHE γ -ray flux above 150 GeV is shown in Fig. 2. There is no evidence of flux variability on a night-by-night basis. A fit with a constant flux of $(6.3 \pm 1.6) \times 10^{-12} \text{ ph cm}^{-2} \text{ s}^{-1}$ resulted in $\chi^2/NDF = 3.5/5$, where NDF stands for number of degrees of freedom. This is equivalent to (2.0 ± 0.5) per cent of the Crab Nebula VHE γ -ray flux. The measured flux is consistent with the UL set by the MAGIC observations of H1722+119 from the previous campaign ([Aleksić et al. 2011](#)). The differential energy spectrum was reconstructed using the Forward Unfolding algorithm presented in [Albert et al. \(2007a\)](#). It can be described by a simple power law function $dN/dE = f_0(E/E_0)^{-\Gamma}$ with normalization $f_0 = (4.3 \pm 0.9_{\text{stat}} \pm 0.9_{\text{syst}}) \times 10^{-11} \text{ ph cm}^{-2} \text{ s}^{-1} \text{ TeV}^{-1}$ and a photon index $\Gamma = 3.3 \pm 0.3_{\text{stat}} \pm 0.2_{\text{syst}}$, at normalization energy $E_0 = 200 \text{ GeV}$.

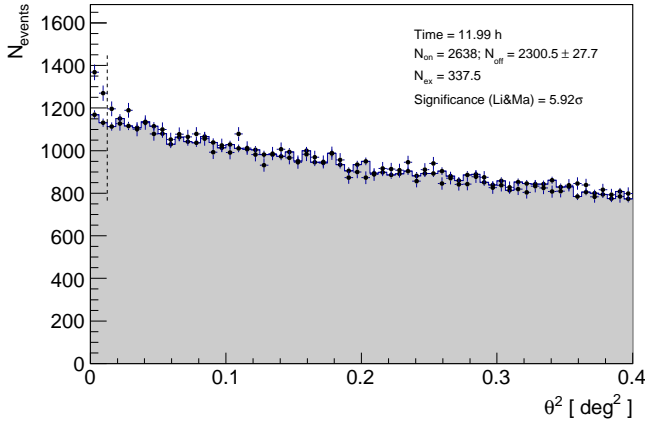


Figure 1. θ^2 distribution of signal (black points) and background (grey area) events. N_{on} is the number of all events with $\theta^2 < 0.0125 \text{ deg}^2$ (vertical dashed line) with respect to the source position in the camera, and N_{off} the normalised number of all events from the same region around OFF-source position.

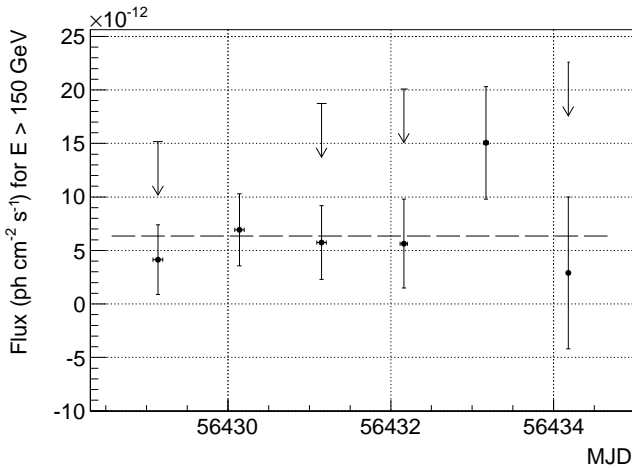


Figure 2. MAGIC nightly light curve for energies above 150 GeV. Horizontal error bars represent the duration of each observation. Vertical arrows represent ULs for points whose relative error of the excess is > 0.5 . The horizontal dashed line is a constant flux fit with parameters stated in the text.

The fit resulted in ($\chi^2/NDF = 3.6/8$). The systematic uncertainty of the photon index was estimated to be ± 0.2 , using Eq. 3 of [Aleksić et al. \(2016b\)](#). We estimate the error on the f_0 to be 20 per cent, which does not include the energy scale uncertainty estimated to be 17 per cent.

2.2 *Fermi*-LAT

The *Fermi*-LAT is a pair-conversion telescope operating from 20 MeV to > 300 GeV. Details about the *Fermi*-LAT are given in [Atwood et al. \(2009\)](#). The LAT data reported in this paper were collected from 2013 January 1 (MJD 56293) to December 31 (MJD 56657). During this time, the *Fermi* observatory operated almost entirely in survey mode. The analysis was performed with the *ScienceTools*

software package version v9r32p5. Only Pass 7 reprocessed events belonging to the ‘Source’ class were used. The time intervals when the rocking angle of the LAT was greater than 52° were rejected. In addition, a cut on the zenith angle ($< 100^\circ$) was applied to reduce contamination from the Earth limb γ rays, which are produced by cosmic rays interacting with the upper atmosphere. The spectral analysis was performed with the instrument response function P7REP_SOURCE_V15 using an unbinned maximum-likelihood method implemented in the tool *gtlike* in the 0.1–100 GeV energy range. Isotropic (*iso_source_v05.txt*) and Galactic diffuse emission (*gll_iem_v05_rev1.fit*) components were used to model the background². The normalizations of both components were allowed to vary freely during the spectral fitting.

We analysed a region of interest of 10° radius centred at the location of H1722+119. We evaluated the significance of the γ -ray signal from the source by means of the maximum-likelihood test statistic $TS = 2 (\log L_1 - \log L_0)$, where L is the likelihood of the data given the model with (L_1) or without (L_0) a point source at the position of H1722+119 (e.g. [Mattox et al. 1996](#)). The source model used in *gtlike* includes all sources from the 3FGL catalogue that fall within 15° of the source. A first maximum-likelihood analysis was performed to remove from the model the sources having $TS < 10$ and/or the predicted number of counts based on the fitted model $N_{\text{pred}} < 3$. A second maximum-likelihood analysis was performed on the updated source model. In the fitting procedure, the normalization factors and the photon indices of the sources lying within 10° of H1722+119 were left as free parameters. For the sources located between 10° and 15° from our target, we kept the normalization and the photon index fixed to the values from the 3FGL catalogue.

All uncertainties in measured HE γ -ray flux reported throughout this paper are statistical only. The systematic uncertainty in the flux is dominated by the systematic uncertainty in the effective area ([Ackermann et al. 2012](#)), which amounts to 5–10 per cent in the 0.1–100 GeV energy range, and therefore smaller than the typical statistical uncertainties for this analysis³.

Integrating over the period 2013 January 1 – December 31 in the 0.1–100 GeV energy range, using a power law model as in the 3FGL catalogue, the fit yielded a $TS = 335$, with an average flux of $(4.1 \pm 0.7) \times 10^{-8} \text{ ph cm}^{-2} \text{ s}^{-1}$, and a photon index of $\Gamma = 1.99 \pm 0.08$ at the decorrelation energy $E_0 = 3063 \text{ MeV}$. During the same period, the fit with a log-parabola model, $dN/dE \propto (E/E_0)^{-\alpha-\beta \log(E/E_0)}$, in the 0.1–100 GeV energy range results in $TS = 355$, with a spectral slope $\alpha = 1.99 \pm 0.08$, and a curvature parameter $\beta = 0.01 \pm 0.01$, indicating no significant curvature of the γ -ray spectrum. The LAT light curve and the photon index evolution with 2-month time bins is shown in [Fig. 3](#). The 2-month bin width is a trade-off between the significance of the source ($TS > 25$ in each time bin) and the shortest time-scale to be probed. For each time bin, the spectral parameters for H1722+119 and for all the sources within 10° from the target were left free to vary. No significant increase of the γ -ray activity was observed by LAT

² fermi.gsfc.nasa.gov/ssc/data/access/lat/BackgroundModels.html

³ fermi.gsfc.nasa.gov/ssc/data/analysis/LAT_caveats.html

in 2013 May and June – the time bin contemporaneous to the MAGIC observations. Both the flux and the photon index are well fitted by a constant with the following parameters: flux: $p_0 = (3.43 \pm 0.56) \times 10^{-8} \text{ ph cm}^{-2} \text{ s}^{-1}$ and $\chi^2/NDF = 3.87/5$, photon index: $\Gamma = 1.96 \pm 0.07$ and $\chi^2/NDF = 1.68/5$. Leaving the photon index free to vary during 2013 May, we obtained $TS = 37$, with an average flux of $(8.5 \pm 3.3) \times 10^{-9} \text{ ph cm}^{-2} \text{ s}^{-1}$, and a photon index of $\Gamma = 1.4 \pm 0.3$. The hint of hardening of the LAT spectrum may be an indication of the shift of the IC peak to higher energies during the MAGIC detection. By considering only the period May 13–26, including the MAGIC observation period, the maximum-likelihood analysis results in a $TS = 15$, with a flux of $(0.9 \pm 0.4) \times 10^{-8} \text{ ph cm}^{-2} \text{ s}^{-1}$ (assuming $\Gamma = 1.4$). By means of the `gtsrcprob` tool, we estimated that the highest energy photon emitted from H1722+119 (with probability > 90 per cent of being associated with the source) was observed on 2013 April 28 (MJD 54610), with an energy of 65.7 GeV. Another photon with an energy 51.6 GeV was observed on 2013 December 31 (MJD 56657).

2.3 Swift

The *Swift* satellite (Gehrels et al. 2004) performed three observations of H1722+119 on 2008 May 31, 2013 January 15 and May 20. The observations were carried out with all three on board instruments: the X-ray Telescope (XRT; Burrows et al. 2005, 0.2–10.0 keV), the Ultraviolet/Optical Telescope (UVOT; Roming et al. 2005, 170–600 nm) and the Burst Alert Telescope (BAT; Barthelmy et al. 2005, 15–150 keV). The hard X-ray flux of this source is below the sensitivity of the BAT instrument for the short exposure of these observations (see Table 1), therefore the data from this instrument are not included in this work. Moreover, the source is not present in the *Swift*/BAT 70-month hard X-ray catalogue (Baumgartner et al. 2013).

The XRT data were processed with standard procedures (`xrtpipeline v0.12.8`), filtering, and screening criteria using the `HEASOFT` package (v6.14). The data were collected in photon counting (PC) mode on 2008 May 31 and 2013 January 15, and windowed timing (WT) mode on 2013 May 20. The source count rate in PC mode was low ($< 0.5 \text{ counts s}^{-1}$); thus pile-up correction was not required. Source events were extracted from a circular region with a radius of 20 pixels (1 pixel = 2.36 arcsec), while background events were extracted from a circular region with a radius of 50 pixels in PC mode and 20 pixels in WT mode away from the source region and from other bright sources. Ancillary response files were generated with `xrtmkarf`, and account for different extraction regions, vignetting and point-spread function corrections. We used the spectral redistribution matrices in the Calibration data base maintained by HEASARC. We fitted the spectrum with an absorbed power law using the photoelectric absorption model `tbabs` (Wilms et al. 2000), with a neutral hydrogen column density fixed to its Galactic value ($N_{\text{H}} = 8.88 \times 10^{20} \text{ cm}^{-2}$; Kalberla et al. 2005). We noted that the X-ray flux of the source observed in 2013, i.e. $(1-2) \times 10^{-11} \text{ erg cm}^{-2} \text{ s}^{-1}$ (Fig. 3), is a factor between 3 and 5 higher than the flux in 2008 May 31, $(3.6 \pm 0.7) \times 10^{-12} \text{ erg cm}^{-2} \text{ s}^{-1}$, with no significant spectral change (Table 1). For the observation in 2013 May 20, with the higher statistics, we fit the spec-

trum also with a log-parabola model, obtaining a spectral slope $\alpha = 2.2 \pm 0.1$, a curvature parameter of $\beta = 0.54_{-0.31}^{+0.34}$, and a $\chi^2_{\text{red}}/NDF = 1.124/63$. The F-test shows an improvement of the fit with respect to the simple power law ($\chi^2_{\text{red}}/NDF = 1.245/64$) with a probability of 99.9 per cent.

UVOT data in the *v*, *b*, *u*, *w1*, *m2*, and *w2* filters were reduced with the `HEASOFT` package v6.16 executing the aperture-photometry task `uvotsource`. We extracted the source counts from an aperture of $5''$ centred on the source, and the background counts from a circle with 10 arcsec radius in a nearby source-free region. Magnitudes were converted into dereddened flux densities by adopting the extinction value $E(B-V) = 0.1497$ from Schlafly & Finkbeiner (2011), the mean Galactic extinction curve in Fitzpatrick (1999) and the magnitude-flux calibrations by Bessell & Brett (1988). The UVOT flux densities collected in 2013 are reported in Fig. 3. The flux densities observed in 2008 May 31 are a factor of 2 lower with respect to the 2013 observations.

Checking the source SED (Fig. 5), we noticed that a monotonic connection between optical-UV and X-ray spectrum was not possible, which motivated us to analyse possible sources of errors affecting the data. An aperture correction procedure was executed for the 2013 May 20 UVOT images in all filters, estimating from field stars the correction to magnitudes extracted with full-width at half maximum (FWHM) radius circular apertures to obtain the counts within the standard apertures ($5''$ radii). A first photometry of the object with apertures of $2.5''$ (the FWHM for all filters) was executed. Then 6 to 8 non-saturated field stars were selected and photometry was performed for each of them using FWHM radii and standard apertures, and non-contaminated background annular regions of radii $26''$ to $33''$. The weighted mean among all magnitude differences obtained with the two different apertures was calculated and finally subtracted from the object magnitude at FWHM apertures. Results are however compatible with the standard procedure, with a low flux in the *w1* filter. Another check was required because the source colour, $b - v \sim 0.7$, is out of the range to which the average count rate to flux ratios (CFR) estimated by Breeveld et al. (2011) are applicable. Therefore, we explored UVOT calibration issues following the procedure described in Raiteri et al. (2010). We fit the source spectrum with a power law and convolved it with the filter effective areas and appropriate physical quantities to derive source-dependent effective wavelengths (EW) and CFR. However, the results obtained are very similar to those given by Breeveld et al., the largest variations being an increase of the EW by 2 and 3 per cent in the *w1* and *w2* band, respectively, and of the CFR by 4 per cent in *w1*. More significant differences were found when comparing the convolved Galactic extinction values with those obtained by simply evaluating them at the filter EW. We obtained a 7 per cent decrease of the extinction in the *w2* and *m2* bands, and an 8 per cent increase in the *w1* band. The optical part of the SED remained essentially unchanged after the re-calibration procedure. The results after the re-calibration procedure are shown in Fig. 5.

Table 1. Log and fitting results of *Swift*/XRT observations of H1722+119 using a power law model with N_{H} fixed to Galactic absorption.

| Observation Date (MJD) | Net Exposure Time s | Photon index Γ | Flux 2-10 keV $\times 10^{-12}$ erg cm $^{-2}$ s $^{-1}$ | χ^2_{red} (<i>NDF</i>) |
|---------------------------|------------------------|--------------------------|---|--------------------------------------|
| 2008-05-31 (54617) | 1733 | 2.13 ± 0.22 | 3.6 ± 0.7 | 1.257 (11) |
| 2013-01-15 (56307) | 812 | 2.28 ± 0.15 | 17.8 ± 2.3 | 0.9040 (17) |
| 2013-05-20 (56432) | 1983 | 2.31 ± 0.08 | 10.5 ± 0.7 | 1.245 (64) |

2.4 KVA

The KVA telescope is located at the Observatorio del Roque de los Muchachos, La Palma (Canary Islands, Spain), and is operated by the Tuorla Observatory, Finland⁴. The telescope consists of a 0.6-m f/15 Cassegrain devoted to polarimetry, and a 0.35-m f/11 Schmidt-Cassegrain auxiliary telescope for multicolour photometry. The telescope has been successfully operated remotely since the fall of 2003. The KVA is used for optical support observations for MAGIC by making R-band photometric observations, typically one measurement per night per source.

H1722+119 has been regularly monitored by the KVA since 2005. At the beginning of May 2013, after an extended optical high state, the source reached an R-band magnitude of 14.65 (flux of 5.96 ± 0.09 mJy), which constituted a historical maximum for this source at that time⁵. The high emission state triggered observations by MAGIC, but the MAGIC observations started during the decreasing part of the optical flaring activity. The KVA observed nightly light curve for 2013 is shown in Fig. 3. The flux varied significantly, the ratio between the highest and lowest flux being 1.6, but we saw no regularity in this variation.

The data were reduced by the Tuorla Observatory Team as described in Nilsson et al. (2016, in prep.). The data were corrected for Galactic extinction using the total absorption $A_{\lambda} = 0.374$ mag from Schlafly & Finkbeiner (2011).

2.5 OVRO

The 40-m radio telescope at the OVRO observes at the 15 GHz band. In late 2007, it started regular monitoring of a sample of blazars in order to support the goals of the *Fermi*-LAT telescope (Richards et al. 2011). This monitoring program includes about 1800 known or potential γ -ray-loud blazars, including all candidate γ -ray blazar survey (CGRaBS; Healey et al. 2008) sources above declination -20° . The sources in this program are observed in total intensity twice per week with a 4 mJy (minimum) and 3 per cent (typical) uncertainty on the flux density. Observations are performed with a dual-beam (each 2.5 arcmin full-width half-maximum) Dicke-switched system using cold sky in the off-source beam as the reference. Additionally, the source is switched between beams to reduce atmospheric variations. The absolute flux density scale is calibrated using observations of 3C 286, adopting the flux density (3.44 Jy) from Baars et al. (1977). This results in about a 5 per cent absolute scale uncertainty, which is not reflected in the plotted

errors in Fig. 3.

The OVRO nightly light curve for 2013 is shown in Fig. 3. Although there is some indication of a short time variability, we fitted the whole sample with a linear function ($F[\text{Jy}] = p_0 + p_1 \times (t - 56300)[\text{MJD}]$) to point out the general trend of increasing flux. The fit parameters are $p_0 = (5.2 \pm 0.2) \times 10^{-2}$ Jy, $p_1 = (1.07 \pm 0.10) \times 10^{-4}$ Jy/day and $\chi^2/NDF = 39.68/36$. We also considered the possibility of a constant flux, but that assumption was discarded with $\chi^2/NDF = 146.9/37$ ($p = 5 \times 10^{-15}$).

3 RESULTS

3.1 Redshift and the intrinsic VHE γ -ray spectrum

VHE γ -rays can be absorbed by the extragalactic background light (EBL), through photon-photon interactions, resulting in e^+e^- pair-production. The flux attenuation is directly dependent on the redshift of the source and energy of γ -rays. A redshift-estimation method described in Prandini et al. (2010) uses this fact. It relies on the assumption that both HE and VHE γ -rays are created by the same physical processes and in the same region, and that the intrinsic spectrum in the VHE range cannot be harder than the spectrum in the HE range. The method uses only the spectral slope of the HE range data. The VHE γ -ray spectrum was de-absorbed using the EBL model from Franceschini et al. (2008). Because spectral points obtained by the MAGIC telescopes at energies below 100 GeV are usually affected by larger systematic uncertainties, they are not used for the fit of the VHE spectrum. The reconstructed redshift is obtained by applying a simple empirical formula to the value estimated from de-absorption. Applying this method to the MAGIC and contemporaneous (2013 May; MJD 56413 – 56442) *Fermi*-LAT data we obtained the reconstructed redshift of H1722+119 to be $z = 0.34 \pm 0.15_{\text{stat}} \pm 0.05_{\text{meth}}$, the error marked as *meth* being a result of the method as described in Prandini et al. (2010). The UL on the redshift was set to 1.06 for the 95 per cent confidence level. Applying the log likelihood ratio test to set the UL, as described in e.g. Mazin & Goebel (2007), we obtained a value of 0.95. When de-absorbed for redshift values greater than 0.95, the spectrum shape becomes parabolic in a $\log(dN/dE)$ vs $\log E$ representation, with apparent minimum at ≈ 200 GeV. Our reconstructed redshift value is in agreement with the latest Landoni et al. (2014) and Farina et al. (2013) results. We used our result combined with the LL from Farina et al. ($z > 0.4$) to de-absorb the VHE γ -ray flux. For $z = 0.4$, and using the EBL model from Franceschini et al. (2008), we found the parame-

⁴ <http://users.utu.fi/kani/1m>

⁵ The highest flux of 7.65 ± 0.11 mJy was measured in 2014 June, and the lowest in 2008 April (2.18 ± 0.05 mJy).

ters of the intrinsic (EBL-deabsorbed) VHE spectrum to be $f_0 = (9.6 \pm 2.2) \times 10^{-11} \text{ ph cm}^{-2} \text{ s}^{-1} \text{ TeV}^{-1}$, $\Gamma = 2.3 \pm 0.4$, $\chi^2/NDF = 3.1/8$.

3.2 Multifrequency light curve

As already mentioned in Section 2.4, MAGIC observations were triggered by an extended optical high state, which was the historical R-band maximum at that time. The VHE γ -ray flux (Fig. 2) is compatible with a constant flux and the previously established UL based on combined data taken over several years. None the less, we cannot reach a firm conclusion on whether the source was flaring in the VHE γ -rays during MAGIC observations or not. Observations performed during six consecutive nights were not sufficient to study a longer term variability. However, we compared the HE γ -ray light curve for the entire year to the optical light curve over period 2013 March 22 to October 05, and the radio light curve over period 2013 January 21 to October 05. The *Fermi*-LAT data were divided into 2-month time bins with the photon index left free to vary (Fig. 3), while each point in the KVA and OVRO light curves represents a single measurement. Comparison of fluxes for the entire period of collected data revealed that the OVRO data show an obvious trend of increasing flux on a time-scale of one year (dashed line in the bottom panel of Fig. 3), while the HE γ -ray flux was consistent with being constant, and the optical flux varied with no apparent regularity. Therefore, we cannot claim any connection between emissions in different energy bands.

3.3 SED modelling

The SED for 2013 May is shown in Fig. 5. Only data contemporaneous to MAGIC observations have been considered for modelling the SED for 2013. On 2013 May 22 (MJD 56434), one observation was performed by the OVRO at 15 GHz. The *Swift* data collected on 2013 May 20 (MJD 56432) were considered, and the R-band observation by the KVA from the same night was used to obtain a spectral point at $4.56 \times 10^{14} \text{ Hz}$. The *Fermi*-LAT spectrum was calculated in the period 2013 May 1 – June 30. The MAGIC spectral points were obtained with Schmelling’s method as described in Albert et al. (2007a). Based on the arguments discussed in Section 3.1, we adopted a value for redshift of 0.4, and EBL model from Franceschini et al. (2008) to get the intrinsic VHE part of the spectrum. We also show the *Swift* data collected on 2008 May 31 (MJD 54617), in order to compare the source SED during the two different brightness states. Archival data from the 2MASS (Two Micron All Sky Survey) All-Sky Catalog of Point Sources (Cutri et al. 2003) and AllWISE (Wide-field Infrared Survey Explorer) Data Release (Cutri & et al. 2013) are included to show the overall behaviour in the IR-optical band, however these were not considered for modelling. We also show the near-IR and optical spectral points from Landoni et al. (2014), which were also not used for modelling.

The source SED shows surprising behaviour in the frequency range $\sim 3 \times 10^{14} - 10^{18} \text{ Hz}$. Indeed, the de-absorbed (as described in Section 2.3) optical–UV spectrum appears curved, with a peak in the *b* band and a steep slope in the

UV. H1722+119 is a bona fide BL Lac type of source. None of the observations used in this work, nor information found in the literature revealed anything about the nature of the black hole environment, nor the host galaxy. There is no evidence of emission at any frequency from the accretion disc, dust torus or BLR. In fact, Landoni et al. (2014) detected no intrinsic or intervening spectral lines, and set the ratio of beamed to thermal emission to be ≥ 400 .

Therefore we do not expect the presence of thermal emission from an accretion disc and the host galaxy that can justify the shape of the optical–UV spectrum. Moreover, this shape prevents a monotonic connection with the X-ray spectrum, as would be expected if both the optical–UV and X-ray emissions were produced by a synchrotron process in the same jet region. The connection between the UV and X-ray spectrum in both states requires an inflection point that is hard to reproduce with simple, one-zone models. This instead can easily be obtained in the framework of a curved jet. Indeed, curved/helical geometries have often been observed in blazar jets (see e.g. Villata & Raiteri 1999, and references therein). A helical-jet morphology can arise as the result of perturbations induced by orbital motion in a binary black hole system or precession of the black hole spin axis (Villata & Raiteri 1999, and references therein; Rieger 2004). 3-D magnetohydrodynamic (MHD) simulations by Nakamura et al. (2001); Moll et al. (2008); Mignone et al. (2010) show how kink instabilities lead to a wiggled, in particular helical, jet structure. MHD equilibrium of helical jets was investigated by Villata & Ferrari (1995).

We adopted the helical jet model originally proposed by Villata & Raiteri (1999) to explain the observed SED variations of Mkn 501, and later applied also to other objects like S4 0954+65 (Raiteri et al. 1999), AO 0235+16 (Ostorero et al. 2004), BL Lacertae (Raiteri et al. 2009; 2010) and PG 1553+113 (Raiteri et al. 2015). The axis of the helical-shaped jet is assumed to lie along the *z*-axis of a 3-D reference frame. The pitch angle is ζ and ψ is the angle defined by the helix axis with the line of sight. The non-dimensional length of the helical path can be expressed in terms of the *z* coordinate along the helix axis:

$$l(z) = \frac{z}{\cos \zeta}, \quad 0 \leq z \leq 1, \quad (1)$$

which corresponds to an azimuthal angle $\varphi(z) = az$, where the angle *a* is a constant. The jet viewing angle varies along the helical path as

$$\cos \theta(z) = \cos \psi \cos \zeta + \sin \psi \sin \zeta \cos(\phi - az), \quad (2)$$

where ϕ is the azimuthal difference between the line of sight and the initial direction of the helical path. The jet is inhomogeneous: each slice of the jet can radiate, in the plasma rest reference frame, synchrotron photons from a minimum frequency $\nu'_{s,\min}$ to a maximum one $\nu'_{s,\max}$, which follow the laws:

$$\nu'_{s,i}(l) = \nu'_{s,i}(0) \left(1 + \frac{l}{l_i}\right)^{-c_i}, \quad c_i > 0, \quad (3)$$

where l_i are length scales, and $i = \min, \max$. The model takes into account IC scattering of the synchrotron photons by the same relativistic electrons emitting them (i.e. SSC). Consequently, each portion of the jet emitting synchrotron radiation between $\nu'_{s,\min}(l)$ and $\nu'_{s,\max}(l)$ will also produce IC radiation between $\nu'_{c,\min}(l)$ and $\nu'_{c,\max}(l)$, with

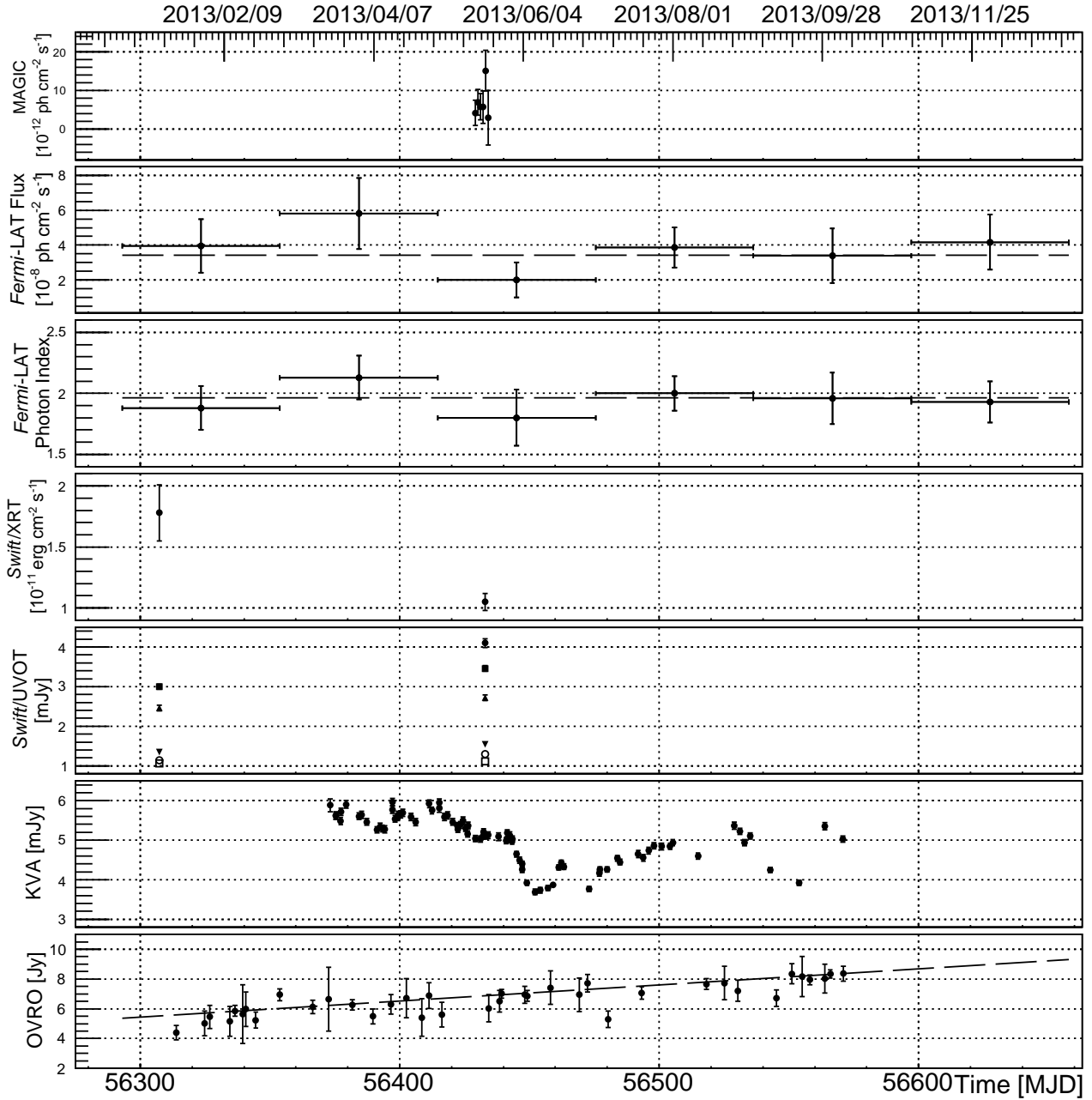


Figure 3. Multifrequency light curve during 2013. MAGIC nightly light curve is the same as in Fig. 2. ULs were omitted for clarity. The HE γ -ray light curve and the evolution of the spectral index, as measured by *Fermi*-LAT, are shown in 2-month time bins, while one night time-scale is used in light curves in other energy bands. Horizontal dashed lines in both panels represent the fit with a constant. The *Swift*/UVOT filters are represented with the following markers: *v* – full circle, *b* – full square, *u* – upward triangle, *w1* – downward triangle, *m2* – empty circle, and *w2* – empty square. The dashed line in the OVRO panel represents a linear function fit. All the fit parameters are given in the text. The data were collected (from top to bottom) by MAGIC ($E > 150$ GeV), *Fermi*-LAT ($0.1 \text{ GeV} < E < 100 \text{ GeV}$), *Swift*/XRT, *Swift*/UVOT, KVA (R-band) and OVRO (15 GHz).

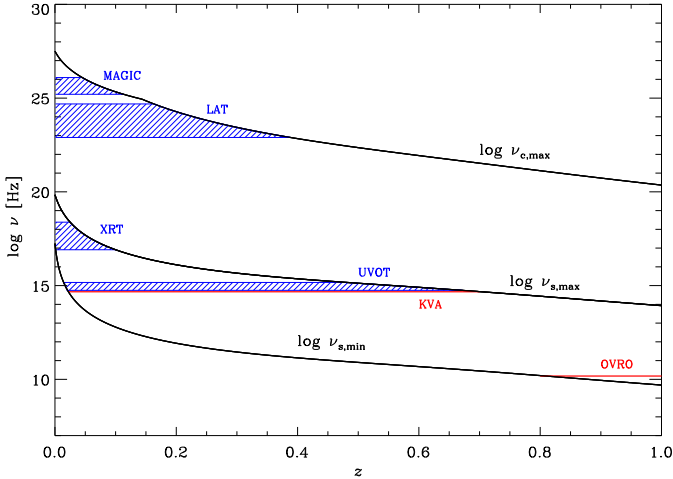


Figure 4. The trend of the observed frequencies as a function of the distance along the helical jet axis z (whose unit length can be estimated to be about 0.1 pc, see text). The location of the regions that contribute to the emission observed by the various instruments is highlighted. The plot refers to the high emission state shown in Fig. 5.

$\nu_{c,i}(l) = \frac{4}{3}\gamma_i^2(l)\nu'_{s,i}(l)$. The electron Lorentz factor ranges from $\gamma_{\min} = 1$ to $\gamma_{\max}(l)$, which has a similar dependence as in Eq. 3, with power c_γ and length scale l_γ . As photon energies increase, the classical Thomson scattering cross section gradually shifts into the extreme Klein-Nishina one, which makes Compton scattering less efficient. In our approximation $\nu'_{c,\max}(l)$ is averaged with $\nu'_{c,\max}(l) = \frac{m_e c^2}{h} \gamma_{\max}(l)$ when $\gamma_{\max}(l)\nu'_{s,\max}(l) > \frac{3}{4}\frac{m_e c^2}{h}$. We assume a power law dependence of the observed flux density on the frequency and a cubic dependence on the Doppler beaming factor δ : $F_\nu(\nu) \propto \delta^3 \nu^{-\alpha_0}$, where α_0 is the power law index of the local synchrotron spectrum, $\delta = [\Gamma_b(1 - \beta \cos \theta)]^{-1}$, β is the bulk velocity of the emitting plasma in units of the speed of light, $\Gamma_b = (1 - \beta^2)^{-1/2}$ the corresponding bulk Lorentz factor, and θ is the viewing angle of Eq. 2. The variation of the viewing angle along the helical path implies a change of the beaming factor. As a consequence, the flux at ν peaks when the part of the jet mostly contributing to it has minimum θ . The emissivity varies along the jet, so that for a jet slice of thickness dl :

$$dF_{\nu,s}(\nu) = K_s \delta^3(l) \nu^{-\alpha_0} \left(1 + \frac{l}{l_s}\right)^{-c_{s1}} \left(\frac{l}{l_s}\right)^{c_{s1}/c_{s2}} dl, \quad (4)$$

$$dF_{\nu,c}(\nu) = K_c \delta^3(l) \nu^{-\alpha_0} \left(1 + \frac{l}{l_c}\right)^{-c_{c1}} \left(\frac{l}{l_c}\right)^{c_{c1}/c_{c2}} \times \ln \left[\frac{\nu'_{s,\max}(l)}{\nu'_{s,\min}(l)} \right] dl, \quad (5)$$

where $c_{s1}, c_{s2}, c_{c1}, c_{c2} > 0$. The observed flux densities at frequency ν coming from the whole emitting jet are obtained by integrating over all the jet portions contributing to that observed frequency (see Fig. 4). Therefore, the observed flux density at each frequency will in general differ depending on the emissivity and beaming of each contributing jet portion, resulting in the overall shape of the SED.

The helical jet model is intended to be a geometrical,

Table 2. Main parameters of the helical model to fit the SEDs of H1722+119. The only difference between the high and low state is the angle ϕ , which changes from 25° to 31° .

| | |
|-------------------------|----------------------|
| ζ | 30° |
| a | 40° |
| ψ | 25° |
| ϕ | $25^\circ, 31^\circ$ |
| α_0 | 0.5 |
| Γ_b | 10 |
| $\log \nu'_{s,\min}(0)$ | 16.7 |
| $\log \nu'_{s,\max}(0)$ | 19.3 |
| $c_{\min,\max}$ | 3.3 |
| $\log l_{\min}$ | -2.3 |
| $\log l_{\max}$ | -1.8 |
| $\log \gamma_{\max}(0)$ | 4.8 |
| c_γ | 1.5 |
| $\log l_\gamma$ | -1 |
| $c_{s1,c1}$ | 3 |
| $c_{s2,c2}$ | 2.3 |
| $\log l_{s,c}$ | -1 |
| $\log K_s$ | -19.25 |
| $\log K_c$ | -24.55 |

dimensionless, model used to describe blazar variability and should not be interpreted as a physical model. However, absolute dimensions can be derived by comparison with VLBA images. In our model, the 15 GHz radio emission comes from the outer 20 per cent of the jet (see Fig. 4). This is assumed to be the jet region where the bulk of the observed 15 GHz radiation comes from. The results of the MOJAVE program⁶ show that the size of the emitting core is $\lesssim 0.1$ pc. Therefore the unit length in our model would correspond to a dimension of the order of one tenth of a parsec.

The helical jet model can produce reasonable fits to the source SEDs (see Fig. 5), although the model applied to 2008 data is only constrained by the synchrotron emission, because there are no contemporaneous data in other energy bands. The noticeable thing is that both fits were obtained with the same choice of model parameters (see Table 2), with the exception of the angle ϕ , which changes from 25° to 31° when going from the high to the low state. This underlines how variations of a few degrees in the viewing angle alone may account for the observed flux changes.

4 SUMMARY AND CONCLUSIONS

MAGIC detected VHE γ -radiation from BL Lac H1722+119 after observations were triggered by a high flux in R-band measured by the KVA. The MAGIC observations were performed during six consecutive nights and show no flux variability. No significant increase of the activity was observed at HE by *Fermi*-LAT in 2013 May neither on short time-scales nor compared to the average 2013 flux. An indication of spectral hardening at HE in 2013 May might explain a VHE γ -ray flux high enough to be detected by the MAGIC telescopes. Changes in flux were significant in optical and radio data. However, on a time-scale of a year, the radio flux seems to increase, while there was no significant variability

⁶ www.physics.purdue.edu/astro/MOJAVE/sourcepages/1722+119.shtml

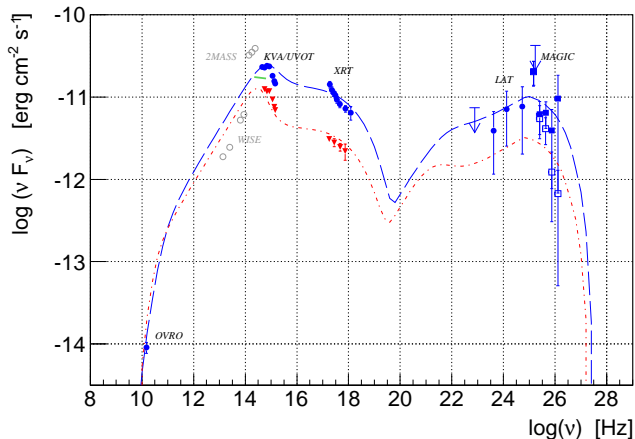


Figure 5. The H1722+119 SED. Blue dots represents data contemporaneous to MAGIC observations. The MAGIC measured data are shown by empty blue squares, while full blue squares indicate the de-absorbed points using the EBL model from Franceschini et al. (2008). *Fermi*-LAT data are shown by dots, while arrows represent *Fermi*-LAT ULs. The *Swift* data indicated by blue dots, were taken on 2013 May 20 (MJD 56432). The KVA R-band point represented by a blue dot was taken on the same night. The OVRO measurement represented by a blue dot was taken on 2013 May 22 (MJD 56434). Red triangles show the *Swift* data from 2008 May 31 (MJD 54617). The green solid line in the $10^{14} - 10^{15}$ Hz range indicates data from Landoni et al. (2014), but they were not considered for the fit. Archival data from 2MASS and WISE are shown by empty grey circles, and were not considered for the fit. The blue long-dashed line indicates fits of the helical jet model to the 2013 data, while the fit to the 2008 data is indicated by the red dash-dot line. Both models represent the intrinsic VHE emission. Only blue and red points were considered for modelling.

of the HE flux. Therefore, we cannot claim that the two components originate from the same physical region. While the radio flux was highest towards the end of the year, the highest optical flux was observed in April, followed by a quite sudden drop, which did not occur in radio data.

The SED shows an interesting feature in the optical–UV band. A break between the optical–UV parts of the spectrum is clearly visible. It also prevents a smooth connection between optical, UV and X-ray bands. We proposed the helical jet model from Villata & Raiteri (1999) to explain the observed emission. We found that the difference between the two states can be attributed to a change of a few degrees in the jet orientation.

Further multifrequency observations will be crucial to investigate in detail this new VHE emitting blazar and its emission mechanisms.

ACKNOWLEDGEMENTS

We are grateful to Marco Landoni for help with adopting data from Landoni et al. (2014).

We would like to thank the Instituto de Astrofísica de Canarias for the excellent working conditions at the Observatorio del Roque de los Muchachos in La Palma. The financial support of the German BMBF and MPG, the Italian

INFN and INAF, the Swiss National Fund SNF, the ERDF under the Spanish MINECO (FPA2012-39502), and the Japanese JSPS and MEXT is gratefully acknowledged. This work was also supported by the Centro de Excelencia Severo Ochoa SEV-2012-0234, CPAN CSD2007-00042, and Multi-Dark CSD2009-00064 projects of the Spanish Consolider-Ingenio 2010 programme, by grant 268740 of the Academy of Finland, by the Croatian Science Foundation (HrZZ) Project 09/176 and the University of Rijeka Project 13.12.1.3.02, by the DFG Collaborative Research Centers SFB823/C4 and SFB876/C3, and by the Polish MNiSzW grant 745/N-HESS-MAGIC/2010/0.

The *Fermi*-LAT Collaboration acknowledges generous ongoing support from a number of agencies and institutes that have supported both the development and the operation of the LAT as well as scientific data analysis. These include the National Aeronautics and Space Administration and the Department of Energy in the United States, the Commissariat à l’Energie Atomique and the Centre National de la Recherche Scientifique / Institut National de Physique Nucléaire et de Physique des Particules in France, the Agenzia Spaziale Italiana and the Istituto Nazionale di Fisica Nucleare in Italy, the Ministry of Education, Culture, Sports, Science and Technology (MEXT), High Energy Accelerator Research Organization (KEK) and Japan Aerospace Exploration Agency (JAXA) in Japan, and the K. A. Wallenberg Foundation, the Swedish Research Council and the Swedish National Space Board in Sweden.

Additional support for science analysis during the operations phase from the following agencies is also gratefully acknowledged: the Istituto Nazionale di Astrofisica in Italy and the Centre National d’Études Spatiales in France.

The OVRO 40-m monitoring program is supported in part by NASA grants NNX08AW31G and NNX11A043G, and NSF grants AST-0808050 and AST-1109911.

Antonio Stamerra acknowledges financial support in the frame of the INAF Senior Scientist program of ASDC and by the Italian Ministry for Research and Scuola Normale Superiore.

Elisa Prandini gratefully acknowledges the financial support of the Marie Heim-Vogtlin grant of the Swiss National Science Foundation.

REFERENCES

- Acero F., et al., 2015, *ApJS*, **218**, 23
 Ackermann M., et al., 2012, *ApJS*, **203**, 4
 Albert J., et al., 2006, *ApJ*, **648**, L105
 Albert J., et al., 2007a, *Nucl. Instrum. Meth. Phys. Res. A*, **583**, 494
 Albert J., et al., 2007b, *ApJ*, **667**, L21
 Albert J., et al., 2008a, *Nucl. Instrum. Meth. Phys. Res. A*, **594**, 407
 Albert J., et al., 2008b, *ApJ*, **681**, 944
 Aleksić J., et al., 2011, *ApJ*, **729**, 115
 Aleksić J., et al., 2012a, *Astroparticle Physics*, **35**, 435
 Aleksić J., et al., 2012b, *A&A*, **539**, A118
 Aleksić J., et al., 2012c, *A&A*, **544**, A142
 Aleksić J., et al., 2014, *A&A*, **563**, A90
 Aleksić J., et al., 2015, *MNRAS*, **451**, 739
 Aleksić J., et al., 2016a, *Astroparticle Physics*, **72**, 61
 Aleksić J., et al., 2016b, *Astroparticle Physics*, **72**, 76
 Anderhub H., et al., 2009, *ApJ*, **704**, L129

- Atwood W. B., et al., 2009, *ApJ*, **697**, 1071
- Baars J. W. M., Genzel R., Pauliny-Toth I. I. K., Witzel A., 1977, *A&A*, **61**, 99
- Barthelmy S., et al., 2005, *Space Sci. Rev.*, **120**, 143
- Baumgartner W. H., Tueller J., Markwardt C. B., Skinner G. K., Barthelmy S., Mushotzky R. F., Evans P. A., Gehrels N., 2013, *ApJS*, **207**, 19
- Bessell M. S., Brett J. M., 1988, *PASP*, **100**, 1134
- Böttcher M., Reimer A., Sweeney K., Prakash A., 2013, *ApJ*, **768**, 54
- Breeveld A. A., Landsman W., Holland S. T., Roming P., Kuin N. P. M., Page M. J., 2011, *AIP Conference Proceedings*, **1358**, 373
- Brissenden R. J. V., Tuohy I. R., Remillard R. A., Schwartz D. A., Hertz P. L., 1990, *ApJS*, **350**, 578
- Burrows D. N., et al., 2005, *Space Sci. Rev.*, **120**, 165
- Cortina J., 2013, The Astronomer's Telegram, **5080**, 1
- Cortina J., et al., 2005, International Cosmic Ray Conference, **5**, 359
- Costamante L., Ghisellini G., 2002, *A&A*, **384**, 56
- Cutri R. M., et al. 2013, VizieR Online Data Catalog, **2328**, 0
- Cutri R. M., et al., 2003, The IRSA 2MASS All-Sky Point Source Catalog, NASA/IPAC Infrared Science Archive. <http://irsa.ipac.caltech.edu/applications/Gator/>
- Donato D., Ghisellini G., Tagliaferri G., Fossati G., 2001, *A&A*, **375**, 739
- Dunlop J. S., McLure R. J., Kukula M. J., Baum S. A., O'Dea C. P., Hughes D. H., 2003, *MNRAS*, **340**, 1095
- Falomo R., Bersanelli M., Bouchet P., Tanzi E. G., 1993, *AJ*, **106**, 11
- Falomo R., Scarpa R., Bersanelli M., 1994, *ApJS*, **93**, 125
- Fitzpatrick E. L., 1999, *PASP*, **111**, 63
- Fomin V. P., Stepanian A. A., Lamb R. C., Lewis D. A., Punch M., Weekes T. C., 1994, *Astropart. Phys.*, **2**, 137
- Forman W., Jones C., Cominsky L., Julien P., Murray S., Peters G., Tananbaum H., Giacconi R., 1978, *ApJS*, **38**, 357
- Franceschini A., Rodighiero G., Vaccari M., 2008, *A&A*, **487**, 837
- Gehrels N., et al., 2004, *ApJ*, **611**, 1005
- Ghisellini G., Tavecchio F., Foschini L., Ghirlanda G., Maraschi L., Celotti A., 2010, *MNRAS*, **402**, 497
- Goebel F., Bartko H., Carmona E., Galante N., Jogler T., Mirzoyan R., Coarasa J. A., Teshima M., 2008, International Cosmic Ray Conference, **3**, 1481
- Griffiths R. E., Wilson A. S., Ward M. J., Tapia S., Ulvestad J. S., 1989, *MNRAS*, **240**, 33
- Healey S. E., et al., 2008, *ApJS*, **175**, 97
- Kalberla P. M. W., Burton W. B., Hartmann D., Arnal E. M., Bajaja E., Morras R., Pöppel W. G. L., 2005, *A&A*, **440**, 775
- Komatsu E., et al., 2011, *ApJS*, **192**, 18
- Landoni M., Falomo R., Treves A., Sbarufatti B., 2014, *A&A*, **570**, A126
- Li T.-P., Ma Y.-Q., 1983, *ApJS*, **272**, 317
- Linford J. D., Taylor G. B., Romani R. W., Helmboldt J. F., Readhead A. C. S., Reeves R., Richards J. L., 2012, *ApJS*, **744**, 177
- Lister M. L., et al., 2011, *ApJS*, **742**, 27
- Lombardi S., K. B., Colin P., Ortega A. D., Klepser S. f. t. M. C., 2011, *International Cosmic Ray Conference*, **3**, 266
- Mao L. S., 2011, *New Astron.*, **16**, 503
- Mattox J. R., et al., 1996, *ApJ*, **461**, 396
- Mazin D., Goebel F., 2007, *ApJ*, **655**, L13
- Mignone A., Rossi P., Bodo G., Ferrari A., Massaglia S., 2010, *MNRAS*, **402**, 7
- Moll R., Spruit H. C., Obergaulinger M., 2008, *A&A*, **492**, 621
- Nakamura M., Uchida Y., Hirose S., 2001, *New Astron.*, **6**, 61
- Nieppola E., Tornikoski M., Valtaoja E., 2006, *A&A*, **445**, 441
- Ostorero L., Villata M., Raiteri C. M., 2004, *A&A*, **419**, 913
- Prandini E., Bonoli G., Maraschi L., Mariotti M., Tavecchio F., 2010, *MNRAS*, **405**, L76
- Raiteri C. M., et al., 1999, *A&A*, **352**, 19
- Raiteri C. M., et al., 2009, *A&A*, **507**, 769
- Raiteri C. M., et al., 2010, *A&A*, **524**, A43
- Raiteri C. M., et al., 2015, *MNRAS*, **454**, 353
- Richards J. L., et al., 2011, *ApJS*, **194**, 29
- Rieger F. M., 2004, *ApJ*, **615**, L5
- Roming P., et al., 2005, *Space Sci. Rev.*, **120**, 95
- Sbarufatti B., Treves A., Falomo R., 2005, *ApJ*, **635**, 173
- Sbarufatti B., Treves A., Falomo R., Heidt J., Kotilainen J., Scarpa R., 2006, *AJ*, **132**, 1
- Schlaflly E. F., Finkbeiner D. P., 2011, *ApJ*, **737**, 103
- Sitarek J., Gaug M., Mazin D., Paoletti R., Tesaro D., 2013, *Nucl. Instrum. Meth. Phys. Res. A*, **258**, 109
- Véron-Cetty M.-P., Véron P., 1993, *A&AS*, **100**, 521
- Villata M., Ferrari A., 1995, *A&A*, **293**, 626
- Villata M., Raiteri C. M., 1999, *A&A*, **347**, 30
- Wilms J., Allen A., McCray R., 2000, *ApJ*, **542**, 914
- Wood K. S., et al., 1984, *ApJS*, **56**, 507
- Zanin R., et al., 2013, *Proceedings of 33rd ICRC*

¹ ETH Zurich, CH-8093 Zurich, Switzerland

² Università di Udine, and INFN Trieste, I-33100 Udine, Italy

³ INAF National Institute for Astrophysics, I-00136 Rome, Italy

⁴ Università di Siena, and INFN Pisa, I-53100 Siena, Italy

⁵ Croatian MAGIC Consortium, Rudjer Boskovic Institute, University of Rijeka, University of Split and University of Zagreb, Croatia

⁶ Saha Institute of Nuclear Physics, 1/AF Bidhannagar, Salt Lake, Sector-1, Kolkata 700064, India

⁷ Max-Planck-Institut für Physik, D-80805 München, Germany

⁸ Universidad Complutense, E-28040 Madrid, Spain

⁹ Inst. de Astrofísica de Canarias, E-38200 La Laguna, Tenerife, Spain; Universidad de La Laguna, Dpto. Astrofísica, E-38206 La Laguna, Tenerife, Spain

¹⁰ University of Łódź, PL-90236 Lodz, Poland

¹¹ Deutsches Elektronen-Synchrotron (DESY), D-15738 Zeuthen, Germany

¹² Institut de Física d'Altes Energies (IFAE), The Barcelona Institute of Science and Technology, Campus UAB, 08193 Bellaterra (Barcelona), Spain

¹³ Universität Würzburg, D-97074 Würzburg, Germany

¹⁴ Università di Padova and INFN, I-35131 Padova, Italy

¹⁵ Institute for Space Sciences (CSIC/IEEC), E-08193 Barcelona, Spain

¹⁶ Technische Universität Dortmund, D-44221 Dortmund, Germany

¹⁷ Finnish MAGIC Consortium, Tuorla Observatory, University of Turku and Astronomy Division, University of Oulu, Finland

¹⁸ Unitat de Física de les Radiacions, Departament de Física, and CERES-IEEC, Universitat Autònoma de Barcelona, E-08193 Bellaterra, Spain

¹⁹ Universitat de Barcelona, ICC, IEEC-UB, E-08028 Barcelona, Spain

²⁰ Japanese MAGIC Consortium, ICRF, The University of Tokyo, Department of Physics and Hakubi Center, Kyoto University, Tokai University, The University of Tokushima, KEK, Japan

²¹ Inst. for Nucl. Research and Nucl. Energy, BG-1784 Sofia, Bulgaria

²² Università di Pisa, and INFN Pisa, I-56126 Pisa, Italy

²³ ICREA and Institute for Space Sciences (CSIC/IEEC), E-08193 Barcelona, Spain

²⁴ Brasileiro de Pesquisas Físicas (CBPF/MCTI), R. Dr. Xavier Sigaud, 150 - Urca, Rio de Janeiro - RJ, 22290-180, Brazil

²⁵ NASA Goddard Space Flight Center, Greenbelt, MD 20771, USA and Department of Physics and Department of Astronomy, University of Maryland, College Park, MD 20742, USA

²⁶ Humboldt University of Berlin, Institut für Physik Newtonstr. 15, 12489 Berlin, Germany

²⁷ Ecole polytechnique fédérale de Lausanne (EPFL), Lausanne, Switzerland

²⁸ Finnish Centre for Astronomy with ESO (FINCA), Turku, Finland

²⁹ INAF – Osservatorio Astronomico di Trieste, Trieste, Italy

³⁰ ISDC - Science Data Center for Astrophysics, 1290, Versoix (Geneva), Switzerland

³¹ Dip. Di Fisica e Astronomia, Università degli Studi di Bologna, I-40127 Bologna, Italy

³² INAF – Istituto di Radioastronomia, I-40129 Bologna, Italy

³³ Aalto University Metsähovi Radio Observatory, Metsähovintie 114, FI-02540 Kylmäla, Finland

³⁴ Cahill Center for Astronomy and Astrophysics, California Institute of Technology, Pasadena, CA 91125, USA

³⁵ National Radio Astronomy Observatory (NRAO), PO Box 0, Socorro, NM 87801, USA

³⁶ INAF – Osservatorio Astrofisico di Torino, I-10025 Pino Torinese (TO), Italy

³⁷ Tuorla Observatory, Department of Physics and Astronomy, University of Turku, Finland

³⁸ Department of Physics, Purdue University, Northwestern Avenue 525, West Lafayette, IN 47907, USA

³⁹ INAF – Osservatorio Astronomico di Roma, I-00040 Monteporzio Catone, Italy

⁴⁰ ASI Science Data Center (ASDC), I-00133 Roma, Italy

This paper has been typeset from a $\text{\TeX}/\text{\LaTeX}$ file prepared by the author.